AGU PUBLICATIONS

Geophysical Research Letters

RESEARCH LETTER
10.1002/2016GL068855

Key Points:
- Short-term solar UV variations produce detectable temperature responses in both the tropical lower stratosphere and troposphere
- The measured temperature responses imply relative downwelling in the tropical lower stratosphere
- The midtropospheric temperature response is most significant in the Pacific sector, especially during the positive phase of ENSO

Supporting Information:
- Supporting Information S1

Correspondence to:
L. L. Hood,
lon@lpl.arizona.edu

Citation:
Hood, L. L. (2016), Lagged response of tropical tropospheric temperature to solar ultraviolet variations on intraseasonal time scales, *Geophys. Res. Lett.*, *43*, 4066–4075, doi:10.1002/2016GL068855.

Received 10 FEB 2016
Accepted 14 APR 2016
Accepted article online 19 APR 2016
Published online 30 APR 2016

Lagged response of tropical tropospheric temperature to solar ultraviolet variations on intraseasonal time scales

L. L. Hood[1]

[1] Lunar and Planetary Laboratory, University of Arizona, Tucson, Arizona, USA

Abstract Correlative and regression analyses of daily ERA-Interim reanalysis data for three separate solar maximum periods confirm the existence of a temperature response to short-term (mainly ~27 day) solar ultraviolet variations at tropical latitudes in both the lower stratosphere and troposphere. The response, which occurs at a phase lag of 6–10 days after the solar forcing peak, consists of a warming in the lower stratosphere, consistent with relative downwelling and a slowing of the mean meridional (Brewer-Dobson) circulation, and a cooling in the troposphere. The midtropospheric cooling response is most significant in the tropical Pacific, especially under positive El Niño–Southern Oscillation conditions and may be related to a reduction in the number of Madden-Julian oscillation events that propagate eastward into the central Pacific following peaks in short-term solar forcing.

1. Introduction

During periods when the presence of active regions on the solar disk combined with solar rotation produces strong variations in ultraviolet spectral irradiance, perturbations of ozone, temperature, and dynamics that are dominantly solar in origin are detectable in the stratosphere [e.g., *Hood*, 1986, 2004]. In addition to direct photochemical production of ozone and radiative heating in the upper stratosphere, associated changes in zonal winds can have indirect effects at lower levels [*Hood and Jirikowic*, 1991; *Ruzmaikin et al.*, 2007; *Garfinkel et al.*, 2015]. In particular, evidence for a slowing of the tropical upwelling rate in the lower stratosphere following short-term solar UV increases [*Hood*, 2003] indicates that solar variability on this time scale is able to modify planetary wave propagation and absorption, leading to a solar-induced perturbation of the mean meridional Brewer-Dobson circulation (BDC).

Here an analysis of 15 years of daily ERA-Interim reanalysis temperature data under solar maximum conditions is reported. The objectives are (a) to refine estimates of the short-term temperature response in the tropical lower stratosphere (related to the tropical upwelling response) and (b) to investigate whether any secondary effects on tropospheric temperature at tropical latitudes are detectable. The method of analysis and correlative results are described in section 2. Results of linear regression analyses to estimate the temperature response to a given increase in solar UV flux and the implied changes in lower stratospheric upwelling rates are described in section 3. In section 4, a possible relationship of the observed tropospheric component of the response to the Madden-Julian oscillation is discussed. A summary and conclusions are given in section 5.

2. Data and Correlative Results

Daily temperature data at 6 h resolution from ERA-Interim [*Dee et al.*, 2011] (available from http://apps.ecmwf.int/datasets) are investigated. In principle, a similar analysis could be performed using lower stratospheric ozone data, but high-quality satellite ozone profile measurements extending into the lower stratosphere are not available for the three solar maximum periods considered here. As a measure of solar UV forcing at wavelengths that directly influence ozone production and radiative heating in the upper stratosphere, the solar spectral irradiance at 205 nm (hereafter F205) estimated using the Naval Research Laboratory (NRL) model [*Lean*, 2000] is chosen (available from http://lasp.colorado.edu/lisird/nrlssi). The 205 nm wavelength is used because it is just short of the Al I edge where variability remains large (up to 4% on solar rotational time scales). However, alternate possible solar variables (e.g., total solar irradiance) are also tested below.

To increase detectability of solar-induced signals and allow empirical verification tests, ERA data from three 5 year intervals centered on solar maxima for cycles 21, 22, and 23 (1979–1983; 1989–1993; and 1999–2003) were selected for detailed analysis. These maxima, especially those of cycles 21 and 22, were relatively strong

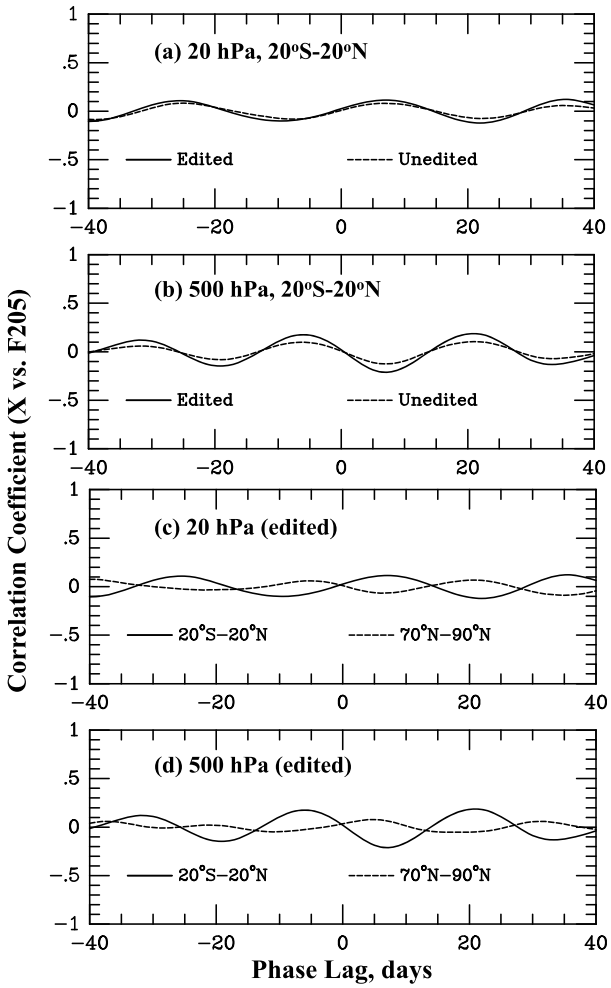

Figure 1. Cross-correlation functions between ERA-Interim zonally averaged temperature deviations and the NRL solar flux at 205 nm for representative pressure levels in the (a, c) lower stratosphere (20 hPa) and (b, d) midtroposphere (500 hPa). In Figures 1a and 1b, comparisons are made for tropical averages before and after editing of the time series to eliminate periods of relatively weak solar UV variations. In Figures 1c and 1d, comparisons are made for edited averages over tropical and north polar latitudes.

and included a large number of variations on solar rotational time scales. As shown in Figures S1 and S2 of the supporting information, short-term F205 variations can be half as large as solar cycle variations and several hundred rotational cycles are available for testing and verifying any identified solar signal. The temperature data, obtained at 1° × 1° spatial resolution, were initially processed to calculate daily area-weighted zonal averages in 1° latitude bands. Following earlier work [e.g., *Hood*, 1986; *Hood and Zhou*, 1998], day-to-day variability was minimized by calculating 5 day running averages of the zonal averages. Then seasonal and longer-term variability was suppressed by calculating deviations of the 5 day running means from 35 day running means. The NRL F205 data set was processed in the same manner as the temperature data. The dependence of the results on the choice of a 35 day upper bound is investigated below by carrying out separate analyses using deviations from 61 day running means. Finally, area-weighted averages of the ERA data from 20°S to 20°N were calculated. Figure S2 compares time series of the processed ERA-Interim tropical averages in the lower stratosphere (70 hPa) and midtroposphere (600 hPa) to the processed F205 series for each of the three 5 year intervals.

To investigate whether a solar signal is detectable in the tropical lower stratosphere and troposphere, cross-correlation functions were calculated (with normalization) at a series of pressure levels. Figure 1 shows results obtained when all three 5 year periods were combined together for two representative levels (20 hPa and 500 hPa). Figure S3 is a similar figure using deviations from 61 day running means. In Figures 1a and 1b,

dashed lines are results when all data are considered, while solid lines are for a selected ("edited") subset of the data during which solar UV variations were relatively large, as indicated in Figure S2. A total of 9 years of measurements out of the original 15 were selected for the edited data set.

Comparing the dashed and solid lines in Figures 1a and 1b, it is seen that the edited data generally produce larger correlations at a given phase lag, as expected if a solar signal is being detected. Correlations are strongest (+0.12 at 20 hPa and −0.21 at 500 hPa) at a phase lag of ~6–10 days after the solar forcing peak. Although low in amplitude, they are statistically significant because of the large effective sample size. The number of observations is $9 \times 365/5 = 657$, where 5 is the length of the running average. Successive 5 day averages of either F205 or ERA temperatures have serial correlation coefficients of less than 0.5, which leads to an estimated effective sample size of $657 \times 0.6 = 394$ [*Bretherton et al.*, 1999, equation (31)]. Conservatively assuming a sample size of 300, the correlation coefficients are significant at 95% confidence [e.g., *Bevington*, 1969]. When 61 day deviations are used (Figures S3a and S3b), similar results are obtained but peak correlation amplitudes are reduced to +0.09 and −0.16, respectively, still significant at >90% confidence. Regardless of the upper bound, correlation amplitudes are consistently larger in the troposphere than in the lower stratosphere. At least in part, this could reflect increased data errors in the lower stratosphere (see Figure S9 for a comparison of ERA-Interim data with National Centers for Environmental Prediction/National Center for Atmospheric Research (NCEP/NCAR) data indicating that data errors can occur in the lower stratosphere). Alternatively, positive feedbacks may amplify the tropospheric response, increasing the ratio of signal to noise. As shown in Figure S4, similar results are obtained at other pressure levels with the largest correlations found in the 20–70 hPa range in the lower stratosphere and in the 200–600 hPa range in the troposphere.

As seen in Figures 1c and 1d, cross-correlation functions in the northern polar region (70°N to 90°N) yield maximum lagged correlations after 6–10 days but with opposite sign to those in the tropics in both the lower stratosphere and the midtroposphere. Similar results are obtained using 61 day deviations (Figures S3c and S3d). In the lower stratosphere, this difference between low and high latitudes is consistent with adiabatic temperature changes produced by a slowing of the BDC following the solar forcing peaks, i.e., relative downwelling in the tropics and relative upwelling at high northern winter latitudes.

Figure S5 shows that correlations in the midtroposphere (500 hPa) are in best agreement between the three 5 year periods when solar UV proxies such as F205 and the 10.7 cm solar radio flux are adopted to represent solar variability. Poor results are obtained when using total solar irradiance (Figure S5a), which penetrates directly into the troposphere but is characterized by relatively minor (<0.1%) variability. Correlations and interperiod consistency are also poor for Galactic cosmic ray flux and for the geomagnetic *Ap* index (an indicator of energetic particle precipitation). Similar results are obtained at pressure levels in the lower stratosphere (Figure S6).

3. Linear Regression Analyses and Implied Upwelling Changes

In order to estimate the response amplitude or sensitivity of ERA-Interim temperature deviations to a given change in F205, multiple linear regression analyses were performed. Only solar and linear trend terms are considered so that temperature deviations $T'(t)$ are assumed to be related to daily F205 deviations by $T'(t) = \beta_{solar} F205'(t) + \beta_{trend} t + r(t)$, where t is time in days, β_{solar} and β_{trend} are regression coefficients, and $r(t)$ is the residual noise term. β_{trend} is usually very small but is calculated for completeness. To account for autocorrelation of the residuals (data minus statistical model), a Cochrane-Orcutt ("prewhitening") transformation is applied [e.g., *Tiao et al.*, 1990]. This procedure adjusts both the temperature time series and the solar and linear trend basis functions to ensure that the residuals are approximately white noise. The daily residuals are significantly autocorrelated so the correction typically reduces coefficients and increases standard error estimates by 10–20%.

Final regression results for zonally and tropically averaged temperature are shown as blue and red symbols with two standard deviation error limits in Figure 2. An enlarged plot of the coefficients focusing on the lower stratosphere and troposphere is given in Figure S7. Regression coefficients are expressed as the change in Kelvin for a change in F205 of 0.6 mW/m^2/nm, representing a relatively strong peak-to-peak variation (Figures S1 and S2). For comparison, green symbols show estimates of the response at upper stratospheric pressure levels taken from an analysis of 22 months of Nimbus 7 Stratosphere and Mesosphere Sounder data by *Hood* [1986] after rescaling to the assumed change in F205. Coefficients in the upper stratosphere approach +0.9 K near the stratopause and decrease gradually to less than +0.1 K in the lower stratosphere.

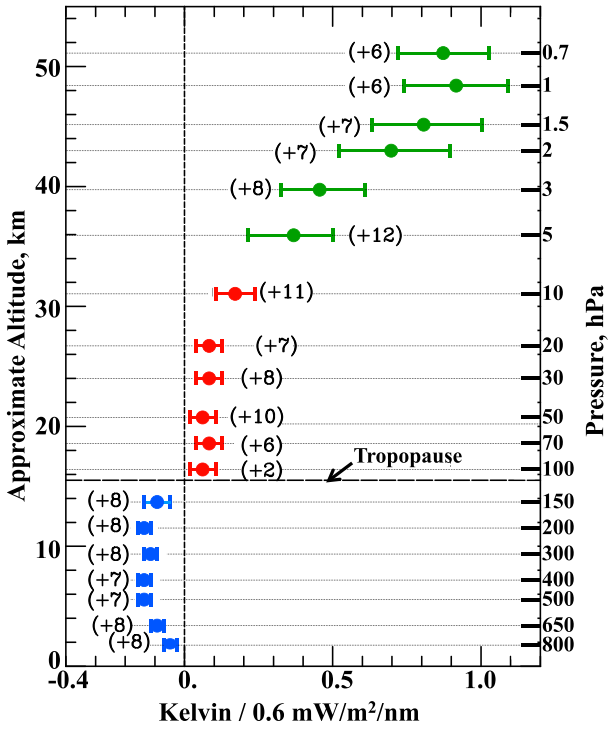

Figure 2. Tropically averaged temperature sensitivity to a change in F205 of 0.6 mW/m^2/nm estimated by linear regression at a series of pressure levels in the stratosphere and troposphere. The phase lag in days when the correlation reached a maximum is shown in parentheses. All time series were processed to minimize variations with periods less than 5 days and greater than 35 days. The green symbols are adapted from *Hood* [1986]. The blue and red symbols are from the present analysis.

In the lower stratosphere and troposphere, the direct effects of solar UV spectral irradiance near 200 nm on ozone production and radiative heating are negligible. It is also unlikely that direct radiative heating at longer wavelengths could contribute significantly to the derived positive lower stratospheric temperature responses plotted in Figure 2. Solar radiation at 250 nm is reduced to $1/e$ of its top-of-atmosphere intensity at an altitude of about 37 km while radiation at 300 nm is reduced to this value at an altitude of 23.5 km [e.g., *Brasseur and Solomon*, 2005, Figure 4.3]. The penetration fraction becomes nearly zero at 70 hPa. Also, while UV radiation varies by as much as 4% on solar rotational time scales near 200 nm, the percentage change is reduced to less than 2% at 250 nm and less than 0.2% at 300 nm [e.g., *Lean*, 1997]. Empirical evidence that radiation near 300 nm is not responsible for the observed temperature response in the lower stratosphere is shown in Figure S8, where it is seen that cross-correlation functions become much less coherent when the NRL 300 nm flux is adopted as the solar forcing variable rather than F205.

A first-order analysis to estimate the vertical velocity changes corresponding to the temperature responses is possible using a simplified version of the thermodynamic energy equation in the Transformed Eulerian Mean (TEM) formulation [e.g., Hood, 2003]. Neglecting meridional heat transport compared to vertical transport and neglecting short-wave heating, this equation can be written as

$$\frac{\partial \overline{T}}{\partial t} \simeq -\overline{w}^{*}(g/c_p) - (\overline{T} - \overline{T}_{\mathrm{eq}})/\tau_r \tag{1}$$

where $\overline{T}$ is zonal mean temperature, $\overline{w}^{*}$ is mean TEM vertical velocity, g/c_p is the dry adiabatic lapse rate ($\simeq$ 9.8 K/km), and where a Newtonian cooling approximation has been assumed with equilibrium temperature $\overline{T}_{\mathrm{eq}}$ and radiative lifetime τ_r. Defining $\overline{T}' = \overline{T} - \overline{T}_{\mathrm{eq}}$ and taking $\overline{T}_{\mathrm{eq}}$ to be approximately constant on these time scales, (1) reduces to $\partial \overline{T}'/\partial t \simeq -\overline{w}^{*}(g/c_p) - \overline{T}'/\tau_r$.

Consider a case in which the observed temperature response in the lower stratosphere is a consequence of changes in $\overline{w}^*$ resulting from "top-down" solar-induced perturbations of the BDC [*Kodera and Kuroda*, 2002; *Nathan and Cordero*, 2007]. Then for short-term UV variations with a dominant ~27 day period, the solar-induced TEM vertical velocity and temperature perturbation can be assumed to be of the form, $\overline{w}^* \simeq \overline{w}_\circ \sin(\omega t)$ and $\overline{T}' \simeq \overline{T}'_\circ \sin(\omega t - \Phi)$, where $\omega = 2\pi/(27 \text{ days})$ and Φ is the phase lag of the temperature maximum relative to the vertical velocity maximum. Substituting into (1), one obtains (see the supporting information for a derivation):

$$\overline{T}'_\circ = -\overline{w}_\circ (g/c_p)\tau_r / \left(1+\omega^2\tau_r^2\right)^{\frac{1}{2}}; \quad \Phi = \tan^{-1}(\omega\tau_r). \tag{2}$$

The effective radiative lifetime in the stratosphere ranges from ~6 days near the stratopause to ~20 days near 10 hPa, increasing to ~100 days by 50 hPa [*Brasseur and Solomon*, 2005]. At 20 hPa where correlative results are shown in Figure 1a, $\tau_r \simeq 30$ days and $\Phi = 0.45\pi$ radians, or about 6 days. The observationally estimated phase lag of zonal mean tropical temperature at this level relative to the solar UV forcing peak is about 7 days. Hence, the implied vertical velocity decrease in the lower stratosphere occurs within a day after the UV forcing peak. Referring to Figure 2 (and Figure S7), the tropical zonal mean temperature response amplitude at 20 hPa for a change in F205 of 0.6 mW/m^2/nm is 0.087 ± 0.044 K. From (2), $\overline{w}_\circ \simeq -(c_p/(g\tau_r))(1+\omega^2\tau_r^2)^{\frac{1}{2}}\overline{T}'_\circ \simeq -0.024 \pm 0.012$ mm/s. Similar results are obtained at other lower stratospheric pressure levels. For comparison, typical vertical velocities in the tropics near 100 hPa are in the range of 0.1 to 0.3 mm/s with a root-mean-square deviation of ~0.15 mm/s [e.g., *Randel et al.*, 2002].

The estimated temperature sensitivities in the troposphere are somewhat larger and more significant than those in the lower stratosphere but are opposite in sign. At 500 hPa, the tropical mean sensitivity to a change in F205 of 0.6 mW/m^2/nm is −0.120 ± 0.024 K at a phase lag of about 7 days (Figures 2 and S7). As will be seen in the next section, this temperature change may reflect differences in diabatic heating rather than differences in upwelling rate. Hence, equation (1) may not be a valid approximation.

Results in the lower stratosphere (red symbols) are qualitatively similar to those of *Hood* [2003] who investigated NCEP-NCAR reanalysis temperature data at pressure levels of 50 to 200 hPa over the 1979–1983 and 1989–1992 periods. However, the amplitude at 100 hPa obtained in that study was increased (~0.24 K), apparently due to anomalous short-term variability near the tropopause in the NCEP-NCAR data (see Figure S9). In both the ERA-Interim reanalysis and the more recent NCEP-Climate Forecast System Reanalysis [*Saha et al.*, 2010], this anomalous behavior is either not present or is greatly reduced in amplitude.

To investigate the dependence of the response on geographic location in the tropics, regression analyses were also performed on temperature deviation time series constructed at each 1° × 1° grid point within the 30°S to 30°N latitude range. Regressions were performed at 12 pressure levels (20, 30, 50, 70, 100, 150, 200, 300, 400, 500, 600, and 800 hPa) and 12 phase lags (−10, −8, −6, −4, −2, 0, +2, +4, +6, +8, +10, and +12 days). As expected from the correlative results of section 2 and the regression results for tropically averaged data of Figure 2, coefficients were most significant with largest amplitudes at positive lags of 6–10 days. Figure 3 shows results at a lag of +8 days for all 12 pressure levels, while Figures S10 and S11 show results at all 12 phase lags for two selected levels, 70 hPa and 600 hPa. In all cases, autocorrelation corrections were applied and regions that are significantly different from zero at more than 2 standard deviations are enclosed by heavy dark lines.

As seen in Figure 3, the response is positive at most longitudes in the lower stratosphere (20 to 70 hPa) with a quasi wave-one structure and a phase that shifts westward with decreasing altitude. Below the tropopause at 150 and 200 hPa, the response becomes dominantly negative and is nearly zonally symmetric. At lower levels, the dependence on longitude becomes more pronounced. At tropical latitudes (20°S to 20°N), the strongest response is obtained at 500 hPa over the south tropical Pacific. The response at this level and at 600 hPa is zonally asymmetric with a large region of statistically significant response over the tropical Pacific. As shown in Figure S12, a pronounced response is obtained over parts of the tropical Pacific at 500 hPa during each of the three edited 5 year solar maximum periods, providing further support for the reality of this characteristic. By 800 hPa, the tropical response is nearly zonally symmetric again and is weaker and less statistically significant. At subtropical latitudes in the midtroposphere, a negative response is obtained in the south Atlantic region (25°N, 330°E), and in the Indian Ocean region (20°N, 50°E). Evidence for at least the south Atlantic response is obtained during all three solar maximum periods (Figure S12).

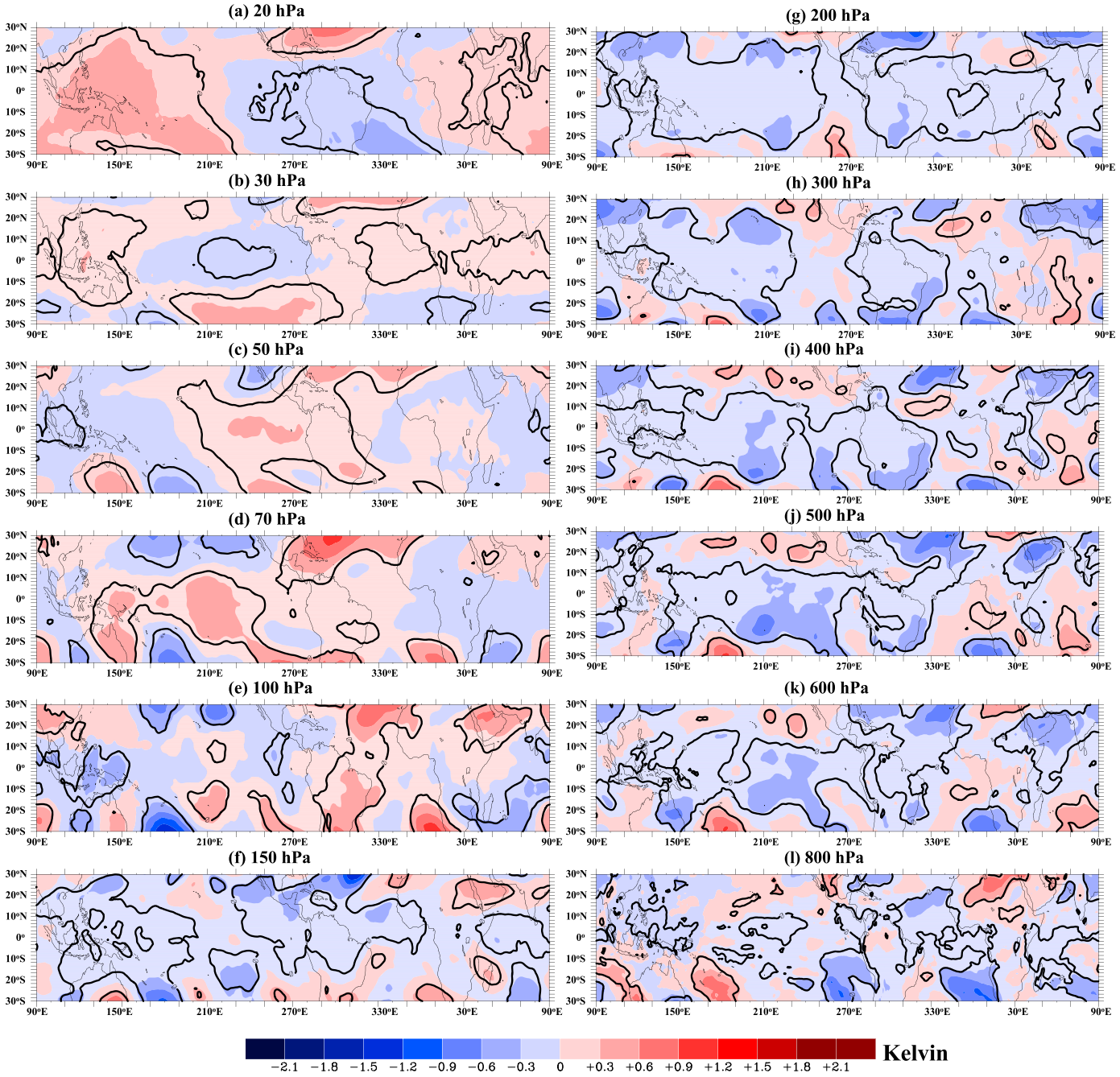

Figure 3. Temperature response to a change in F205 of 0.6 mW/m^2/nm estimated by linear regression at a series of pressure levels for a phase lag of +8 days. Heavy dark lines enclose regions that are formally significant at the 2σ (95% confidence) level.

As shown in Figure S13, the geographically dependent regression results in the midtroposphere are not strongly dependent on the choice of calculating deviations from 35 day running means. Results are nearly the same and are even stronger in the central tropical Pacific when 61 day deviations are used instead of 35 day deviations.

To indicate visually the extent to which solar UV forcing correlates with midtropospheric temperature at regional scales, Figure S14 shows example time series at 500 hPa within the south tropical Pacific region (0°S to 20°S, 200°E to 270°E) where negative temperature responses are consistently significant and strong (Figure 3j). In this region, cross-correlation functions yield a maximum negative correlation of $R = -0.24$ at a

lag of about +10 days when all 9 years of edited solar maximum data are considered. When individual edited periods (identified in Figure S2) are considered, correlation coefficients at +10 days range from −0.14 to −0.34.

Finally, an initial investigation was conducted of the dependence of the tropical regression results on season and on the phase of the El Niño–Southern Oscillation (ENSO). The seasonal analyses were inconclusive, due in part to the large reduction in degrees of freedom when only edited data from 3 months of each year were considered. However, as shown in Figure S15, it was found that the tropical Pacific region of statistically significant response is much larger during the positive (El Niño) ENSO phase than during the negative (La Niña) phase, as determined by the sign of the Niño 3.4 index. A similar investigation of the dependence of the results on the phase of the stratospheric quasi-biennial wind oscillation (QBO) would be straightforward. The QBO significantly modifies the mean state so nonlinear effects may be expected. However, this is deferred to future work.

4. Possible Relationship to the MJO

Several aspects of the correlative and regression results reported here suggest that the inferred tropospheric temperature decreases following solar UV increases are associated with the effects of tropical deep convection. First, as shown in Figures 3j and 3k, the observed negative temperature response is strongest over a large area of statistical significance in the tropical Pacific. Second, as shown in Figure S15, the Pacific response depends on the phase of ENSO with larger amplitude and significance area when the Niño 3.4 index is positive than when it is negative. Several previous studies of sea level pressure and sea surface temperature data on the 11 year time scale have also reported evidence for solar signals in the tropical Pacific [e.g., *van Loon and Meehl*, 2008; *Roy and Haigh*, 2010; *Ruzmaikin and Aumann*, 2012; *Hood et al.*, 2013].

In addition to ENSO, which is a standing oscillation of the atmosphere-ocean system, it is well known that intraseasonal oscillations also exist, the strongest of which is the Madden-Julian oscillation (MJO) [*Madden and Julian*, 1972]. The MJO is an eastward propagating pattern of convective systems, associated rainfall, and latent heat release with a period of ~30–70 days. It is initiated in the Indian Ocean and has largest amplitude in the warm-pool region of the maritime continent, becoming weaker or nonexistent in the central and eastern Pacific [e.g., *Zhang*, 2005]. It has a number of derivative effects on extratropical circulation and intraseasonal weather and climate but remains poorly simulated in most general circulation models [*Hung et al.*, 2013; *DeMott et al.*, 2015].

During a positive ENSO event, the warming of the eastern tropical Pacific extends the warm-pool region eastward, allowing deeper penetration of MJO activity into the central Pacific (see, e.g., the review by *Zhang* [2005]). One possible hypothesis for explaining the central Pacific cooling response in the midtroposphere is therefore that the eastward propagation of the MJO is modulated by solar forcing. Figure 4 shows results of an initial investigation of this hypothesis. As found originally by *Wheeler and Hendon* [2004], the eastward propagation of the MJO can be described as consisting of a series of eight phases with phases 7, 8, and 1 resulting in enhanced precipitation and latent heat release at or east of the dateline (see their Figure 8). Figures 4a and 4b show histograms of the number of occurrences of phases 7, 8, or 1 MJO events as a function of phase lag from key dates marking peaks and minima of the 5–35-day filtered solar flux at 205 nm. The MJO phase data are obtained from http://ds.data.jma.go.jp/tcc/tcc/products/clisys/mjo/figs/olr0-sst1_1980-2010/rmm8.csv, and days when the MJO amplitude was <1 are neglected. Only F205 peaks and minima with absolute values >0.1 mW/m^2/nm are considered. As seen in the figure, during the first 5–7 days after peak dates, the occurrence rate is reduced relative to that at later times while the opposite is true following minima dates. A reduced rate of occurrence of MJO events in the central Pacific following solar peaks will produce a relative cooling because of reduced latent heat release in the midtroposphere. Although the phase lag of the temperature response (6–10 days) is somewhat later than that of the MJO phase response, the occurrence rate results of Figure 4 may not be directly comparable to the 5–35 day filtered cross-correlation and regression results of Figures 1–3 because the MJO phase construction effectively concentrates the variance to periods between 30 and 80 days [*Wheeler and Hendon*, 2004, p. 1919]. In any case, the reduced number of events following solar peak dates and the increased number of events following solar minima dates is qualitatively consistent with this hypothesis.

Several previous observational and modeling studies have found evidence for an influence of stratospheric conditions near the tropical tropopause on deep convection and the MJO. *Giorgetta et al.* [1999] conducted experiments using a general circulation model (GCM) for different phases of the QBO to show that tropical

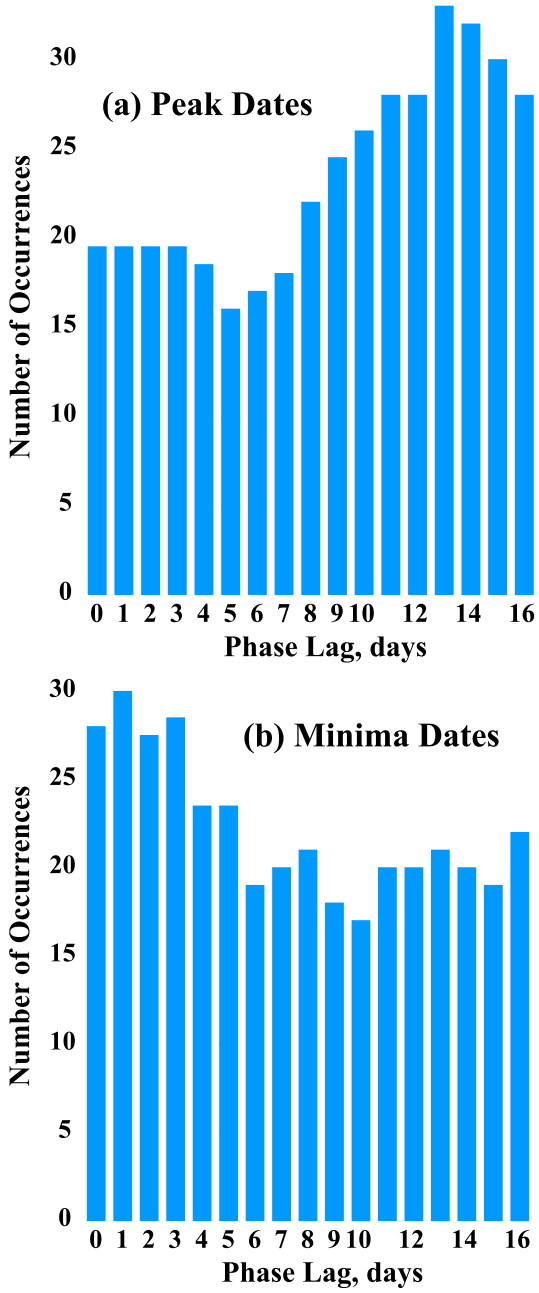

Figure 4. (a) Number of MJO phase 7, 8, 1 events at a series of lags relative to dates when the 5–35 day filtered solar flux at 205 nm reached a peak (95 peak days during 1980–1983; 1989–1993; 1999–2003). Inactive MJO days (MJO amplitude <1) are neglected. (b) As in Figure 4a but relative to dates when F205 reached a minimum (90 minimum days).

tropopause temperatures were higher under westerly QBO conditions. This was explained as due to increased adiabatic heating caused by the induced QBO meridional circulation [*Plumb and Bell*, 1982]. Under westerly QBO conditions, the GCM experiments also yielded a reduction in tropospheric latent heat release and cloud cover, which led to a positive feedback in the form of increased longwave heating at the tropopause. They therefore proposed that the QBO-induced temperature modification near the tropopause and the associated change in static stability was responsible for modifying the vertical scale and therefore the intensity of tropical deep convection. A recent observational study by *Yoo and Son* [2016] has shown that the overall MJO amplitude during northern winter is significantly weaker during the westerly phase of the stratospheric QBO than during the easterly phase. They further present evidence for a negative correlation between MJO amplitude

and thermal stratification (static stability) in the upper troposphere and lower stratosphere, which would be consistent with the mechanism proposed by *Giorgetta et al.* [1999].

Although the above results pertain primarily to an influence of the stratospheric QBO on deep cumulus convection and the MJO, it is possible that the same basic mechanism may be involved in producing a solar influence. Increased adiabatic heating in the tropical tropopause region following solar UV maxima will increase static stability and may therefore also negatively perturb deep tropical convection and the MJO, resulting in a net cooling response and decreased cloud heights in the troposphere. Positive feedbacks from increased longwave heating in the lowermost stratosphere would amplify the response, especially in the Pacific sector where the largest cooling response is obtained in the midtroposphere (Figure 3j). The largest warming response in the lowermost stratosphere (70 hPa) is also found in the same sector (Figure 3d) and reaches an amplitude of ∼0.4 K, which is comparable to QBO-induced zonal mean temperature changes near the tropopause [e.g., *Randel and Cobb*, 1994].

5. Summary and Conclusions

As found in section 2, the reality of the solar UV-induced temperature responses identified here in both the tropical lower stratosphere and midtroposphere is supported by (a) increased correlations when edited data are used (Figures 1a and 1b); and (b) approximate consistency of cross-correlation functions when each of the three 5 year periods is separately analyzed (Figures S5 and S6). Consistent correlations are obtained only when UV proxies are adopted as the solar forcing variable. A similar phase lag of the temperature response (6–10 days) is obtained in both the lower stratosphere and troposphere but the response has a different sign (cooling) in the troposphere. As shown in section 3, regression analyses yield a tropical mean temperature response to a large solar rotational UV variation of 0.05–0.1 K in the tropical lower stratosphere and ∼ −0.12 K in the midtroposphere. Regional responses are as large as +0.3–0.5 K in the lower stratosphere and −0.3–0.5 K in the troposphere. The implied peak-to-peak reductions in tropical mean upwelling rate in the lower stratosphere are of the order −0.02 mm/s.

The tropical tropospheric temperature response has not been previously identified to the author's knowledge. It is zonally symmetric in the upper troposphere and could, in principle, be caused by increases in upwelling rate at these levels. But it is stronger and more significant in the Pacific region in the midtroposphere, especially when the Niño 3.4 index is in its positive phase. The latter characteristics suggest that positive feedbacks involving tropical deep convection, cloudiness, and latent heat release may assist in amplifying both the lower stratospheric and tropospheric responses. Initial investigation of the dependence of MJO eastward propagation on phase lag relative to peaks and minima in short-term solar forcing (Figure 4) supports this possibility.

Acknowledgments
The ERA-Interim temperature data analyzed here are available from http://apps.ecmwf.int/datasets and the NRL 205 nm model solar fluxes are available from http://lasp.colorado.edu/lisird/nrlssi. Thanks to Greg Hopp and Judith Lean for providing the NRL model total solar irradiance data used in Figures S5 and S6. The MJO phase data since 1980 are available from: http://ds.data.jma.go.jp/tcc/tcc/products/clisys/mjo/figs/olr0-sst1_1980-2010/rmm8.csv. Very useful criticisms that significantly improved the paper were provided by two anonymous reviewers, one of whom suggested the analysis that led to Figure 4. Supported by grant NNX14AD44G from the NASA Living With a Star program.

References

Bevington, P. R. (1969), *Data Reduction and Error Analysis for the Physical Sciences*, McGraw-Hill, 336 pp., New York.
Brasseur, G., and S. Solomon (2005), *Aeronomy of the Middle Atmosphere*, Springer, 644 pp., Dordrecht, Netherlands.
Bretherton, C. S., M. Widmann, V. P. Dymnikov, J. M. Wallace, and I. Bladé (1999), The effective number of spatial degrees of freedom of a time-varying field, *J. Clim.*, *12*, 1990–2009.
Dee, D. P., et al. (2011), The ERA-Interim reanalysis: Configuration and performance of the data assimilation system, *Q. J. R. Meteorol. Soc.*, *137*, 553–597.
DeMott, C. A., N. P. Klingaman, and S. J. Woolnough (2015), Atmosphere-ocean coupled processes in the Madden-Julian oscillation, *Rev. Geophys.*, *53*, 1099–1154, doi:10.1002/2014RG000478.
Garfinkel, C. I., V. Silverman, N. Harnik, C. Haspel, and Y. Riz (2015), Stratospheric response to intraseasonal changes in incoming solar radiation, *J. Geophys. Res. Atmos.*, *120*, 7648–7660, doi:10.1002/2015JD023244.
Giorgetta, M. A., L. Bengtsson, and K. Arpe (1999), An investigation of QBO signals in the east Asian and Indian monsoon in GCM experiments, *Clim. Dyn.*, *15*, 435–450, doi:10.1007/s003820050292.
Hood, L. L. (1986), Coupled stratospheric ozone and temperature responses to short-term changes in solar ultraviolet flux: An analysis of Nimbus 7 SBUV and SAMS data, *J. Geophys. Res.*, *91*, 5264–5276.
Hood, L. L. (2003), Thermal response of the tropical tropopause region to solar ultraviolet variations, *Geophys. Res. Lett.*, *30*, 2215, doi:10.1029/2003GL018364.
Hood, L. L. (2004), Effects of solar UV variability on the stratosphere, in *Solar Variability and its Effect on Climate, Geophys. Monogr.*, vol. 141, pp. 283–304, AGU, Washington, D. C.
Hood, L. L., and J. L. Jirikowic (1991), Stratospheric dynamical effects of solar ultraviolet variations: Evidence from zonal mean ozone and temperature data, *J. Geophys. Res.*, *96*, 7565–7577.
Hood, L. L., and S. Zhou (1998), Stratospheric effects of 27-day solar ultraviolet variations: An analysis of UARS MLS ozone and temperature data, *J. Geophys. Res.*, *103*, 3629–3638.
Hood, L., S. Schimanke, T. Spangehl, S. Bal and U. Cubasch (2013), The surface climate response to 11-yr solar forcing during northern winter: Observational analyses and comparisons with GCM simulations, *J. Clim.*, *26*, 7489–7506.

Hung, M.-P., J.-L. Lin, W. Wang, D. Kim, T. Shinoda, and S. J. Weaver (2013), MJO and convectively coupled equatorial waves simulated by CMIP5 climate models, *J. Clim.*, *26*, 6185–6214.
Kodera, K., and Y. Kuroda (2002), Dynamical response to the solar cycle, *J. Geophys. Res.*, *107*, 4749, doi:10.1029/2002JD002224.
Lean, J. (1997), The sun's variable radiation and its relevance for earth, *Ann. Rev. Astron. Astrophys.*, *35*, 33–67.
Lean, J. (2000), A decadal solar effect in the evolution of the Sun's spectral irradiance since the Maunder Minimum, *Geophys. Res. Lett.*, *27*, 2425–2428, doi:10.1029/2000GL000043.
Madden, R. A., and P. R. Julian (1972), Description of global-scale circulation cells in the tropics with a 40–50 day period, *J. Atmos. Sci.*, *29*, 1109–1123.
Nathan, R. R., and E. C. Cordero (2007), An ozone-modified refractive index for vertically propagating planetary waves, *J. Geophys. Res.*, *112*, D02105, doi:10.1029/2006JD007357.
Plumb, R. A., and R. C. Bell (1982), A model of the quasi-biennial oscillation on an equatorial beta-plane, *Q. J. R. Meteorol. Soc.*, *108*, 335–352.
Randel, W. J., and J. B. Cobb (1994), Coherent variations of monthly mean total ozone and lower stratospheric temperature, *J. Geophys. Res.*, *99*, 5433–5447.
Randel, W. J., R. Garcia, and F. Wu (2002), Time-dependent upwelling in the tropical lower stratosphere estimated from the zonal-mean momentum budget, *J. Atmos. Sci.*, *59*, 2141–2152.
Roy, I., and J. Haigh (2010), Solar cycle signals in sea level pressure and sea surface temperature, *Atmos. Chem. Phys.*, *10*, 3147–3153.
Ruzmaikin, A., and H. H. Aumann (2012), Decadal variability of tropical Pacific temperature in relation to solar cycles, *Adv. Space Res.*, *49*, 572–578.
Ruzmaikin, A., M. L. Santee, M. J. Schwartz, L. Froidevaux, and H. Pickett (2007), The 27-day variations in stratospheric ozone and temperature: New MLS data, *Geophys. Res. Lett.*, *34*, L02819, doi:10.1029/2006GL028419.
Saha, S. M., et al. (2010), The NCEP Climate Forecast System Reanalysis, *Bull. Am. Meteorol. Soc.*, *91*, 1015–1057.
Tiao, G., G. Reinsel, D. Xu, J. Pedrick, X. Zhu, A. Miller, J. DeLuisi, C. Mateer, and D. Wuebbles (1990), Effects of autocorrelation and temporal sampling schemes on estimates of trend and spatial correlation, *J. Geophys. Res.*, *95*, 20,507–20,517.
van Loon, H., and G. A. Meehl (2008), The response in the Pacific to the Sun's decadal peaks and contrasts to cold events in the Southern Oscillation, *J. Atmos. Sol. Terr. Phys.*, *70*, 1046–1055.
Wheeler, M. C., and H. H. Hendon (2004), An all-season real-time multivariate MJO index: Development of an index for monitoring and prediction, *Mon. Weather Rev.*, *132*, 1917–1932.
Yoo, C., and S.-W. Son (2016), Modulation of the boreal wintertime Madden-Julian oscillation by the stratospheric quasi-biennial oscillation, *Geophys. Res. Lett.*, *43*, 1392–1398.
Zhang, C. (2005), Madden-Julian Oscillation, *Rev. Geophys.*, *43*, RG2003, doi:10.1029/2004RG000158.